

High-energy excitonic effects in single-layer graphene

Eri Widiyanto ^{1,2} Lucky Zaehir Maulana ³ Edi Suharyadi,² Angelo Giglia,⁴ Konstantin Koshmak,⁴ Stefano Nannarone,⁴ Andriwo Rusydi,^{5,6,*} and Iman Santoso ^{2,†}

¹*Department of Physics, Faculty of Engineering, Universitas Singaperbangsa Karawang, Telukjambe Timur, Karawang 41361, Indonesia*

²*Department of Physics, Faculty of Mathematics and Natural Sciences, Universitas Gadjah Mada, Sekip Utara PO Box BLS 21, Yogyakarta 55281, Indonesia*

³*Department of Physics, Faculty of Science and Technology, Universitas Jambi, 36361, Indonesia*

⁴*CNR-Istituto Officina Materiali, I-34149 Trieste, Italy*

⁵*Advanced Research Initiative for Correlated-Electron Systems (ARICES), Department of Physics, National University of Singapore, 2 Science Drive 3, Singapore 117551, Singapore*

⁶*Singapore Synchrotron Light Source, 5 Research Link, Singapore 117603, Singapore*



(Received 24 August 2023; accepted 15 May 2024; published 6 June 2024)

Using high-energy polarization-dependent reflectivity, we discover high-energy resonant excitons at room temperature in single-layer graphene. The resonant excitons occur at ~ 10.04 and ~ 12.29 eV arising from transitions between parallel σ and π^* states along Γ - K as well as σ and σ^* states at the M point, respectively. The observation of spectral weight transfer signifies electronic correlation and that the two-dimensional nature and low-energy properties are strongly coupled with high-energy bands. Our result shows the importance of electron-electron and electron-hole interactions in determining electronic and optical properties of graphene and two-dimensional systems.

DOI: [10.1103/PhysRevMaterials.8.065201](https://doi.org/10.1103/PhysRevMaterials.8.065201)

I. INTRODUCTION

Electronic correlation is believed to play an important role in determining exotic properties, such as high- T_c superconductivity and colossal magnetoresistance, in two-dimensional (2D) and strongly correlated electron systems in general. Photons of high optical energies are the key to probe electronic correlation and the origin of 2D nature properties in graphene. Graphene, since it was discovered in 2004, has generated significant attention in the global research community due to its exotic quantum properties. The sp^2 hybridized carbon atoms form a one-atom-thick honeycomb structure, and its electrons and holes follow the 2D Dirac equation, exhibiting an unusual linear dispersion band structure at the K point of the Brillouin zone [5,6]. The investigation of electron-electron (e - e) and electron-hole (e - h) systems is crucial for exploring many-body quantum phenomena [4,7-9]. They both dominate the optical response of correlated electron systems affecting their binding, relaxation processes, and other physical properties [10], while the investigation of high-energy excitons and electronic correlation in graphene remain hotly discussed [11,12].

Theoretical studies using the *ab initio* many-body perturbation based on the *GW* approximation and Bethe-Salpeter equation (BSE) approach have predicted and emphasized the significance of electronic correlation resulting in resonant excitonic phenomena in the optical absorption of graphene

[13,14]. Theoretical calculations have predicted resonant excitonic effects in which, depending on the correlation effect, their excited states could generate a series of resonant excitons due to the unique band structures in graphene [13-16]. Experimentally, resonant exciton at 4.6 eV has been observed and attributed to (e - h) interaction in the π and π^* bands at the M point [17-27]. These effects were observed in broadly resonant excitonic states comprising π and π^* bands within the low-energy range (< 10 eV), with short lifetimes and no binding energy. However, it remains a discrepancy with regard to optical properties beyond 10 eV [11,14,16], which require us to reveal electronic correlation.

Theoretical calculations at the higher-energy range have suggested that if many-body correlations are involved, then graphene generally would have been predicted to generate high-energy resonant excitonic effects even up to ~ 20 eV [16]. Importantly, many-body effects connect between high-energy bands and low-energy properties [1,2]. The role of electronic correlations, i.e., electron-electron (e - e) and electron-hole (e - h) interactions, in graphene and 2D systems in general remains hotly debated [13,14,16]. Based on theoretical and recent experimental studies, high-energy optical properties are the key to distinguishing correlation effects in graphene [16] and 2D systems [4].

Furthermore, previous optical measurements were frequently conducted on isolated free-standing graphene, which is usually very tiny and thus needs extensive experimental consideration [22-28]. Our study aims to fill this gap by investigating the optical properties of chemical vapor deposition (CVD) graphene, which is produced using a low-cost method that is compatible with chip fabrication and can yield large-area samples up to 100 m long [29]. By studying the

*andriwo.rusydi@nus.edu.sg

†iman.santoso@ugm.ac.id

high-energy optical properties of graphene, we hope to address the outstanding, fundamental problem on electronic correlation and improve our understanding of its electronic structure and potential applications. Moreover, the ability to regulate the polarization-dependent optical response of graphene is crucial for controlling the interaction between graphene and light, which is essential for the progress of novel optoelectronic devices based on graphene. Modifying the polarization of light allows for the targeted stimulation of various electronic states in graphene, as well as regulation of the material’s absorption, transmission, and reflection of light [30–38].

In this paper, we report high-energy resonant excitons due to many-body correlation effects in single-layer CVD graphene on SiO₂/Si substrate. Due to weak interaction with the substrate, the single-layer CVD graphene is free-standing-like [17,25,27], and supported with theoretical calculations, these optical properties are the 2D nature of graphene. The free-standing-like graphene is different than previous studies where graphene-substrate interactions have been found to play fundamental roles in modifying the optical response and electronic interactions of graphene [27,39–45]. The nature of the interface contributes to the carrier density and work function of graphene, which are fundamental properties for optoelectronics devices [46,47]. Therefore, it is crucial to investigate free-standing graphene or weakly graphene-substrate interaction. We examine the polarization-dependent complex dielectric function and loss function of single-layer graphene within the 9–40 eV energy range. Surprisingly, the high-energy resonant excitonic effects show strong polarization between *s* and *p* polarization. The existence of high-energy resonant excitons reveals the importance of *e–e* and *e–h* interactions in free-standing graphene and the low-energy bands are tightly connected with high-energy bands. This implies that one has to understand and treat graphene as a correlated system rather than that of a noncorrelated or weakly correlated system.

II. EXPERIMENT DETAILS

Single-layer CVD graphene on 1 × 1 cm² SiO₂ (~285 nm)/Si substrate (SKU 1ML-SIO2-5P) was purchased from Graphene Laboratories Inc, Graphene Supermarket, US. The graphene coverage of this product is about 95%, with a sheet resistance of 660–1500 Ω/square. Optical micrograph and Raman spectra of single-layer CVD graphene are recorded using a 532-nm laser excitation wavelength (Micro Confocal Hyperspectral 3D Imaging Raman Spectrometer, LabRAM HR Evolution-HORIBA).

The optical reflectivity of single-layer graphene was measured using a vacuum ultraviolet (VUV) reflectivity at IOM-CNR synchrotron beamline BEAR (bending magnet for emission absorption and reflectivity) at Elettra (Trieste, Italy) using *s*- and *p*-polarized light with the near-normal incident angle of 15° [48]. The measurement was done at room temperature at an ultrahigh vacuum pressure better than 10^{−9} mbar. Fig. 1 shows the analysis results, showing the fitted reflectivity of each sample compared to the measured values. In general, the fitted reflectivity of each sample closely matches its corresponding measured reflectivity. The overall

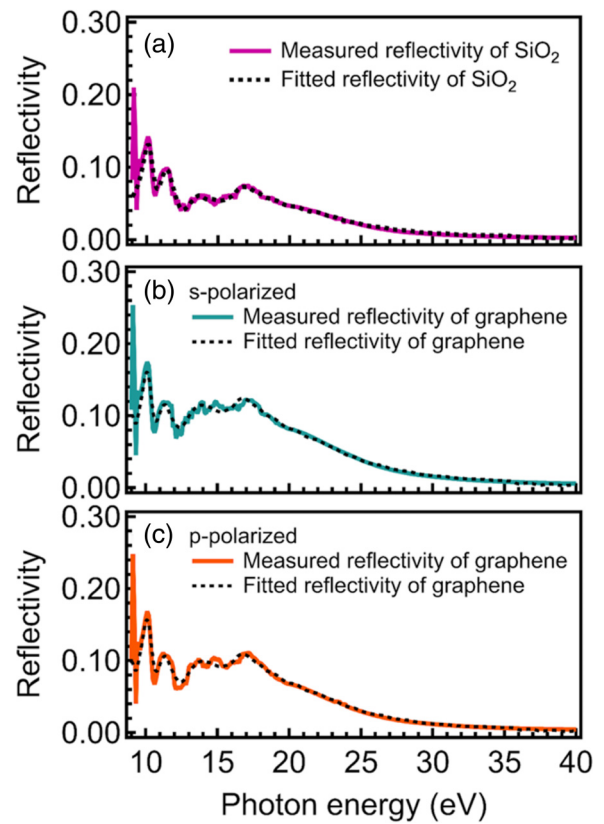


FIG. 1. Fitted reflectivity of each sample as compared to its experimentally measured data: (a) SiO₂/Si substrate, (b) single-layer CVD graphene *s* polarized, and (c) single-layer CVD graphene *p* polarized.

mean squared error (MSE or χ^2) of the fit is 0.09, which is less than 1, indicating an excellent fitting result.

The optical constants are obtained by modeling the system with Fresnel coefficients for an optical multilayered film system, depicted in Fig. 2. The model is composed of a silicon bulk (layer 5), a 285-nm SiO₂ layer (layer 4), a 0.335-nm graphene layer (layer 2), and the air (layer 0). Since the multilayer graphene follows the step morphology of SiO₂, we include additional layer 1 and layer 3 as effective layers to represent the roughness at both the surface of the multilayer graphene and the interface between the multilayer graphene and the substrate.

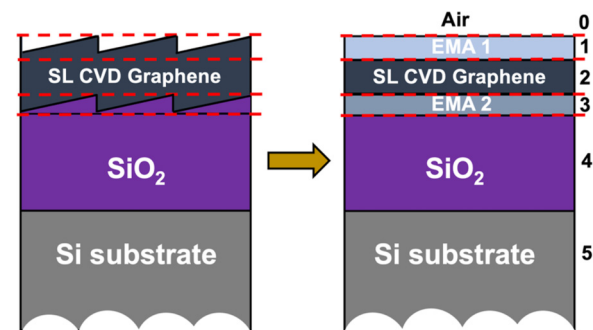


FIG. 2. Optical model of single-layer CVD graphene on SiO₂/Si substrate.

We use the Bruggemann effective medium approximation (EMA), which is comprised of 50% air and 50% graphene, to describe layer 1. For layer 3, we use EMA consisting of 50% graphene and 50% SiO₂. A more common problem is the general sample structure, which consists of n layers on a substrate with $(n + 1)$ interfaces. In order to provide a solution, depicted in Fig. 2, the 2×2 scattering matrix represented by \mathbf{S}_ν is derived, where ν denotes either p or s polarization. This matrix is given by [49]

$$\mathbf{S}_{\nu,6} = \mathbf{I}_{\nu,01} \mathbf{L}_1 \mathbf{I}_{\nu,12} \mathbf{L}_2 \dots \mathbf{I}_{\nu,45} \mathbf{L}_5 \mathbf{I}_{\nu,56} \mathbf{L}_6, \quad (1)$$

where \mathbf{I} and \mathbf{L} are interface matrices and layer matrices. The interface and layer matrices are given by

$$\mathbf{I}_{\nu,(j-1),j} = \frac{1}{t_{\nu,(j-1),j}} \begin{pmatrix} 1 & r_{\nu,(j-1),j} \\ r_{\nu,(j-1),j} & 1 \end{pmatrix}, \quad (2a)$$

$$\mathbf{L}_j = \begin{bmatrix} \exp(-i\beta_j) & 0 \\ 0 & \exp(i\beta_j) \end{bmatrix}, \quad (2b)$$

where $\beta = (\frac{2\pi d}{\lambda}) N_j \cos \theta_j$ is the phase difference between the reflected light at the interface between layer 0 and layer 1, and d is the thickness of the thin film at a specific wavelength λ . In the interface matrix, $r_{\nu,(j-1),j}$ can be calculated using the following formulas [49]:

$$(r_{j-1,j})_p = \frac{N_j \cos \theta_{j-1} - N_{j-1} \cos \theta_j}{N_j \cos \theta_{j-1} + N_{j-1} \cos \theta_j}, \quad (3a)$$

$$(r_{j-1,j})_s = \frac{N_{j-1} \cos \theta_{j-1} - N_j \cos \theta_j}{N_{j-1} \cos \theta_{j-1} + N_j \cos \theta_j}, \quad (3b)$$

These equations represent the reflection (r) coefficients for the interface between layers $j-1$ and j . The total reflectance of the polarized light for the optical model described by Fig. 2 is given by

$$R = R_p \cos^2(P) + R_s \sin^2(P), \quad (4)$$

with R_p , R_s , and P denoting the reflectance of p -polarized light, the reflectance of s -polarized light, and the polarization angle, respectively. R_p and R_s are given by

$$R_p = |r_{012345,p}|^2 \quad \text{and} \quad R_s = |r_{012345,s}|^2, \quad (5)$$

where $r_{012345,p}$ and $r_{012345,s}$ are the reflection coefficients for p - and s -polarized light, respectively. The Fresnel coefficients of reflected light for each interface of two adjacent layers are given by [49]

$$r_{01,p} = \frac{\sqrt{\varepsilon_1} \cos \theta_0 - \sqrt{\varepsilon_0} \cos \theta_1}{\sqrt{\varepsilon_1} \cos \theta_0 + \sqrt{\varepsilon_0} \cos \theta_1}, \quad (6)$$

$$r_{01,s} = \frac{\sqrt{\varepsilon_0} \cos \theta_0 - \sqrt{\varepsilon_1} \cos \theta_1}{\sqrt{\varepsilon_0} \cos \theta_0 + \sqrt{\varepsilon_1} \cos \theta_1}, \quad (7)$$

where we have implicitly applied the Fresnel equation for the interface between medium 0 (air) and medium 1 (EMA) in deriving Eqs. (6) and (7). The p and s denote the p and s polarization of light, respectively. The ε_0 and ε_1 represent the dielectric constant of medium 0 and medium 1, respectively. Here, θ_0 and θ_1 represent the incident and refracted angles at the interface between medium 0 and medium 1, respectively. These angles are related to each other by Snell's law. The Fresnel coefficients of reflected light for other interfaces (e.g., r_{11} and r_{23}) can be obtained by substituting the index

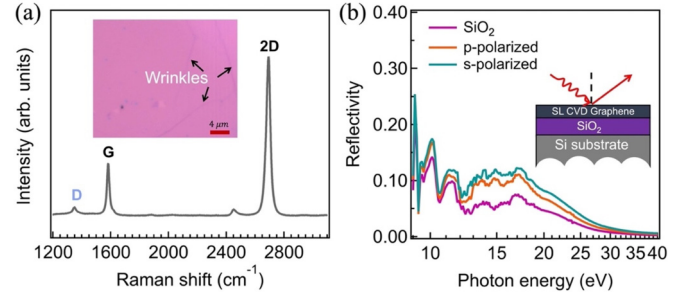


FIG. 3. (a) Raman shift of single-layer graphene. The inset shows an optical micrograph of single-layer graphene with some wrinkles. (b) Reflectivity measurements (s and p polarized) of graphene and SiO₂/Si substrate. Inset: A sketch shows the optical model of the reflectivity experiment at high energy (9–40 eV).

0 and 1 in Eqs. (6) and (7) with the respective index under consideration. The dielectric constants of single-layer CVD graphene and SiO₂/Si substrate are extracted from a fit of the reflectivity data (R) of the overall system and the substrate with the stratified optical model given in Fig. 1. In extracting these dielectric constants, we use oscillators which can be described by the Drude-Lorentz model [49]:

$$\varepsilon(\omega) = \varepsilon_\infty + \sum_k \frac{\omega_{p,k}^2}{\omega_{0,k}^2 - \omega^2 - i\gamma_k \omega}, \quad (8)$$

where ε_∞ denotes the high-energy dielectric constant, representing the contribution from all oscillators at very high energies compared to the energy ranges under examination. The parameters $\omega_{p,k}$, $\omega_{0,k}$, and γ_k are the plasma energy, the transverse energy (eigenenergy), and the linewidth (scattering rate), respectively, of the k th Lorentz oscillator. We take the reflectivity spectrum of a substrate as a reference and do the fitting with the phenomenological oscillators constrained with the Kramers-Kronig transformation. The optical conductivity, $\sigma_1(\omega)$ is related to the imaginary part (or absorption) of the dielectric constant $\varepsilon_2(\omega)$ by the equation

$$\sigma_1(\omega) = \frac{\omega \varepsilon_2(\omega)}{4\pi}. \quad (9)$$

III. RESULTS AND DISCUSSION

The Raman spectra of graphene reveal the characteristic G and 2D bands at 1581 and 2692 cm⁻¹, respectively, with a weak peak-related defect (D band) also present at 1346 cm⁻¹, as shown in Fig. 3(a). The ratio of the intensities of the 2D to G bands (I_{2D}/I_G) is approximately 2, and the 2D band exhibits a symmetric single Lorentzian shape, confirming the presence of single-layer graphene in our sample. Fig. 3 (b) presents the measured reflectivity of each sample. The fitted reflectivity of each sample is matched closely to its respective measured reflectivity (see Fig. 1). Our significant finding is the high-energy reflectivity observed in single-layer graphene, particularly at s and p polarizations, compared to the SiO₂/Si substrate, as illustrated in Fig. 3(b). The reflectivity of graphene is found to be polarization dependent and is significantly higher than that of SiO₂. Significant differences

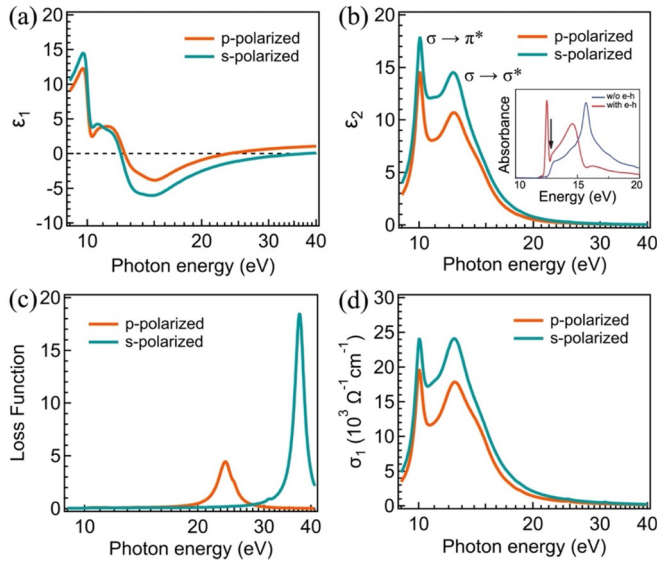


FIG. 4. Experimental polarization-dependent measurement of single-layer graphene: (a) The real part of the dielectric constant (ϵ_1). (b) The imaginary part of the dielectric constant (ϵ_2). The inset shows optical absorption spectra with and without $e-h$ interaction of graphene using first-principles calculations from Ref. [16]. (c) The loss function. (d) The real part of the optical conductivity (σ_1).

in reflectivity exist between the substrate and graphene samples, particularly at high photon energy ranges 9–40 eV.

The procedure for obtaining the complex dielectric constant ($\tilde{\epsilon} = \epsilon_1 + i\epsilon_2$) of single-layer graphene involves modeling the sample with Fresnel coefficients for an optical multilayered film (see Fig. 2), following the approach described in Refs. [50,51]. While previous experimental studies [21,52] have identified resonant excitonic effects within the photon energy range of up to ~ 8 eV, our study reveals new excitonic effects well above it.

The real ϵ_1 [Fig. 4(a)] and imaginary ϵ_2 [Fig. 4(b)] parts of the dielectric function of single-layer graphene show a strong polarization dependence. We reveal two types of excitonic effects: (i) a broad, widely resonant excitonic that reshapes the single-particle interband absorption peak but does not shift the absorption edge, and (ii) a sharp resonant exciton below the continuum. Both types of excitons have comparable optical absorption, resulting in a unique double-peak characteristic that is consistent with previous theoretical predictions [16]. These two excitonic states have energies of approximately ~ 10.04 and ~ 12.29 eV, respectively, and correspond to transitions between parallel σ and π^* states and σ and σ^* states, as shown in the band structure of free-standing graphene in Ref. [16].

We compare our experimental data with first-principles calculations of optical absorbance reported in Ref. [16] to determine the origin of both peak excitons. The inset graph in Fig. 4(b) shows that the optical absorption spectra of graphene exhibit a significant peak around 12–20 eV related to the nearly parallel σ and π^* states and their high joint density of states (JDOS), without $e-h$ interactions. The peak is broadened since these bands are not exactly parallel. Interestingly, the optical absorption spectra of graphene change dramatically accompanied with spectral weight transfer in a broad

energy range even well above 20 eV when $e-e$ and $e-h$ interactions are included, resulting in two optically bright excited states: the prominent exciton with an energy of approximately ~ 12.54 eV and a widely resonant excitonic state with an energy of around ~ 13.75 eV, while the interband transitions above ~ 15 eV are dramatically suppressed [16]. Remarkably, as shown in Fig. 4(b), the line shape between our experimental data and the first-principles calculations from Ref. [16] is very similar, providing conclusive evidence of the 2D nature of resonant excitons due to strong $e-e$ and $e-h$ interactions in graphene.

Our other significant observation is high-energy plasmons seen in the loss function (LF) [Fig. 4(c)]. The LF is calculated using $\text{LF}(\omega) = -\text{Im}[\tilde{\epsilon}^{-1}(\omega)] = \epsilon_2(\omega)/\epsilon_1^2(\omega) + \epsilon_2^2(\omega)$. For sub-x-ray photons, the photon momentum transfer q is finite but approaches zero, and the distinction between longitudinal (l) and transverse (t) $\epsilon(\omega)$ vanishes, that is, $\lim_{|q| \rightarrow 0} \epsilon_l(\mathbf{q}, \omega) = \epsilon_t(\mathbf{q}, \omega)$, allowing us to probe both optical and plasmonic properties in the low- q limit [4,9]. The LF peaks occur at ~ 23.7 and ~ 37.3 eV.

The optical conductivity (σ_1) of single-layer graphene as a function of the imaginary part (or absorption) of the complex dielectric constant (ϵ_2), shown by the equation $\sigma_1 = \omega\epsilon_2/4\pi$, is depicted in Fig. 4(d). Fig. 4 demonstrates that the optical absorption of graphene is highly influenced by the polarization of the incident light. Generally, the absorption and scattering of s -polarized light are greater than those of p -polarized light. The electronic bands in graphene exhibit high anisotropy, meaning that they possess different properties in different directions. When, on the one hand, linearly polarized light with its electric field vector parallel to the graphene plane (s polarization) is incident on graphene, the response is mainly from the σ electron of graphene, which is a linear combination of the $s-p_x$ and $s-p_y$ orbitals. On the other hand, when linearly polarized light with its electric field vector perpendicular to the graphene plane (p polarization) is incident on graphene, the response is primarily from the π electron of graphene, which comes from the p_z orbital of carbon atoms. Due to a finite incident angle, the incoming electric field vector for this polarization is reduced. Therefore, this could lead to the smaller differences between s and p reflectivity observed in our data because there is no reducing the electric field vector for s polarization.

Theoretical calculations based on density-functional theory have been used to investigate graphene on bare Si substrate [53]. When positioned near Si (111) and (100) surfaces, carbon atoms in graphene can form covalent interactions with Si atoms. On the Si (111) surface, the Fermi level of graphene shifts, leading to a three-orders-of-magnitude increase in electron density. The work function of graphene on this surface also increases by 0.29 eV, likely due to the surface dipole caused by the redistribution of π orbitals. The interaction between graphene and the Si surface modifies the number of available states below the Fermi level, resulting in significant changes in electron density and work function [53]. The remarkable rise in charge density observed is attributed to an unconventional n -type doping mechanism, which modifies the DOS instead of transferring charges. The shift of the Fermi level towards the conduction band is higher than both the Dirac point of graphene and the top of the valence band of

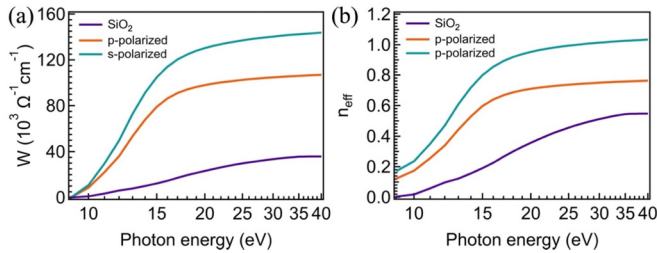


FIG. 5. (a) Spectral weight transfer. (b) The amount of charge redistribution of single-layer graphene on SiO₂.

Si. One possible explanation is that the interaction between the graphene and Si surface reduces the number of available states of both graphene and Si below the Dirac point [53].

The effect of the substrate on the resonant exciton properties of single-layer graphene on SiO₂/Si substrates is evaluated by looking at their respective spectral weight (W). Figs. 5(a) and 5(b) depict the spectral weight analysis of graphene compared with SiO₂ in the area related to the change of the absorption features. The spectral weight $W = \int_{E_1}^{E_2} \sigma_1 dE$ is derived for finite energy ranges to estimate the transfer of charge carriers for different energy regions. At an energy range 9–15 eV, whereas resonant excitons occur, the W for graphene is much bigger than that of W for SiO₂, revealing that the large spectral weight is from graphene and further supporting the important role of electronic correlations. There might be a local bonding between substrate and graphene, which may cause a shift of the resonant exciton peaks [11,53], however, electronic correlations remain dominant. It is worth noting that the optical properties of single-layer graphene are different than that of epitaxial graphene on a 6H-SiC(0001)/buffer layer, which is not a free-standing graphene and has high-energy resonant exciton at ~ 6.3 eV [11], while the optical properties of graphene on quartz are much closer to the theoretical calculations based on GW -BSE [16]. This strongly suggests that the quartz substrate has less effect on the optical properties of graphene, making it free-standing-like graphene.

Figures 6(a) and 6(b) show the decomposition of the room-temperature universal optical conductivity ($\pi e^2/2h$) of single-layer graphene for s and p polarizations. We fit the optical conductivity spectra with the Lorentz model (blue), which can be associated with interband transition and two Fano-shaped vibration modes (purple and green). The Fano

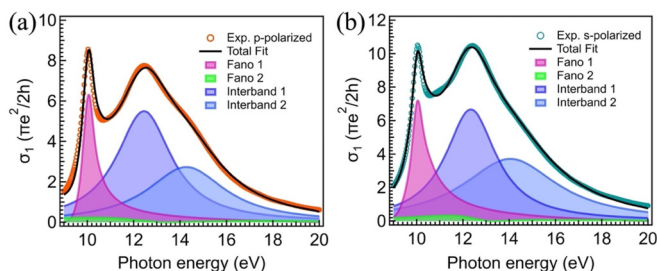


FIG. 6. Decomposition of the room-temperature optical conductivity of single-layer graphene: (a) p polarized and (b) s polarized. The black curve represents the overall spectrum fit with two Fano resonances (purple and green) and two interband transitions (blue).

TABLE I. Fano and Lorentz parameters of single-layer CVD graphene.

Parameters	s polarized	p polarized
Fano 1:		
q	1.94	2.26
Γ	1.49	0.89
E_0	9.81	9.84
E_{res}	10.04	10.09
Fano 2:		
q	-0.68	-0.44
Γ	2.62	5.36
E_0	12.39	12.28
E_{res}	12.87	12.84
Lorentz 1:		
A	12.41	12.53
ω_0	14.84	14.07
Γ	2.67	2.88
Lorentz 2:		
A	14.26	14.41
ω_0	16.17	12.65
Γ	4.97	4.08

line shape indicates coupling (or resonance) between a discrete state and a continuum of electronic states within the same energy range [52,54]. In our case, this coupling occurs between a discrete excitonic state, resulting from e - h interactions, and a continuum of the electronic band structure.

The presence of this Fano resonance can be described by the formula [25] $\sigma_1/\sigma_{1,\text{cont}} = (q + \varepsilon)^2/1 + \varepsilon^2$, where $\sigma_{1,\text{cont}}$ represents the continuum contribution to σ_1 , possibly affected by e - e interactions, and $\varepsilon = 2(\omega - E_{\text{res}})/\Gamma$, where Γ is the lifetime-related width of an exciton and E_{res} is the resonance energy. The line shape is determined by q and q^2 is the ratio of the intensity of the excitonic transition to the unperturbed band-to-band transition. Figures 6(a) and 6(b) display the best fit of σ_1 for s and p polarizations using the Fano analysis and Lorentz model, with the parameters tabulated in Table I.

The optical conductivity spectrum displays a unique double-peak behavior due to the comparable optical absorption of both excitons. This differs from the spectra of bulk metals, 1D metallic carbon nanotubes [55–57], and semiconductors, where excitons either thoroughly wash out the absorption spectrum [58], remain unchanged, or are dominated by resonant excitons [59]. Conventionally, low-energy excitonic effects (electron-hole interactions) are important in determining the optical responses of semiconductors and associated renewable energy applications. In conventional semiconductors such as Si, the binding energy of the bound exciton is ~ 10 meV binding energy, which has a lifetime of ~ 6.6 ns, while in graphene we estimate that the binding energy and the lifetime of resonant exciton at ~ 10.04 eV are ~ 100 meV and ~ 65.8 ns (from the Fano model). These resonant exciton binding energy and its lifetime are significantly larger and longer than Si semiconductors. Based on GW -BSE [16], the calculated binding energy of resonant exciton in graphene is ~ 270 meV, which is close to our experimental data, while the binding energy of the low-energy

resonant exciton for metallic carbon nanotubes is $\sim 30 - 50$ meV [56–58].

IV. CONCLUSIONS

In conclusion, we observe room temperature high-optical-energy resonant excitons in single-layer CVD graphene. These optical properties are the 2D nature of graphene and occur due to electron-electron and electron-hole interactions. Our result calls for further investigations of high-energy optics and electronic correlation in graphene and 2D semimetals as correlated electron systems and opens opportunities in optoelectronic applications by utilizing high-energy optical properties of 2D semimetals.

ACKNOWLEDGMENTS

This work was supported by Kementerian Riset Teknologi Dan Pendidikan Tinggi Republik Indonesia, through Hibah KLN (Grant No. 015/SP2H/LT/DRPM/II/2016). The experiments at BEAR beamline-ELETTRA (Trieste, Italy) were conducted under Proposal No. 20155463. Badan Riset dan Inovasi Nasional partly supported the analysis work (RIIM under Contract No. 12/II.7/HK/2023). EW particularly would like to thank Universitas Gadjah Mada for supporting the post-doctoral program 2024 (No. 4292/UN1.P1/PT.01.03/2024). The work at the National University of Singapore was supported by the Ministry of Education of Singapore (MOE) AcRF Tier-2 (Grants No. MOE-T2EP50220-0018 and No. T2EP50122-0028).

-
- [1] H. Eskes, M. B. J. Meinders, and G. A. Sawatzky, Anomalous transfer of spectral weight in doped strongly correlated systems, *Phys. Rev. Lett.* **67**, 1035 (1991).
- [2] A. Rusydi *et al.*, Metal-insulator transition in manganites: Changes in optical conductivity up to 22 eV, *Phys. Rev. B* **78**, 125110 (2008).
- [3] P. Phillips, Colloquium: Identifying the propagating charge modes in doped Mott insulators, *Rev. Mod. Phys.* **82**, 1719 (2010).
- [4] T. J. Whitcher *et al.*, Unravelling strong electronic interlayer and intralayer correlations in a transition metal dichalcogenide, *Nat. Commun.* **12**, 6980 (2021).
- [5] A. K. Geim and K. S. Novoselov, The rise of graphene, *Nat. Mater.* **6**, 183 (2007).
- [6] A. H. Castro Neto, F. Guinea, N. M. R. Peres, K. S. Novoselov, and A. K. Geim, The electronic properties of graphene, *Rev. Mod. Phys.* **81**, 109 (2009).
- [7] D. A. Bandurin, A. Principi, I. Y. Phinney, T. Taniguchi, K. Watanabe, and P. Jarillo-Herrero, Interlayer electron-hole friction in tunable twisted bilayer graphene semimetal, *Phys. Rev. Lett.* **129**, 206802 (2022).
- [8] D. N. Basov, M. M. Fogler, A. Lanzara, F. Wang, and Y. Zhang, Colloquium: Graphene spectroscopy, *Rev. Mod. Phys.* **86**, 959 (2014).
- [9] T. C. Asmara *et al.*, Tunable and low-loss correlated plasmons in Mott-like insulating oxides, *Nat. Commun.* **8**, 15271 (2017).
- [10] H. Katow, R. Akashi, Y. Miyamoto, and S. Tsuneyuki, First-Principles study of the optical dipole trap for two-dimensional excitons in graphene, *Phys. Rev. Lett.* **129**, 047401 (2022).
- [11] I. Santoso *et al.*, Observation of room-temperature high-energy resonant excitonic effects in graphene, *Phys. Rev. B* **84**, 081403(R) (2011).
- [12] K. F. Mak, L. Ju, F. Wang, and T. F. Heinz, Optical spectroscopy of graphene: From the far infrared to the ultraviolet, *Solid State Commun.* **152**, 1341 (2012).
- [13] L. Yang, J. Deslippe, C. H. Park, M. L. Cohen, and S. G. Louie, Excitonic effects on the optical response of graphene and bilayer graphene, *Phys. Rev. Lett.* **103**, 186802 (2009).
- [14] P. E. Trevisanutto, M. Holzmann, M. Côté, and V. Olevano, Ab initio high-energy excitonic effects in graphite and graphene, *Phys. Rev. B* **81**, 121405(R) (2010).
- [15] L. Yang, Excitonic effects on optical absorption spectra of doped graphene, *Nano Lett.* **11**, 3844 (2011).
- [16] L. Yang, Excitons in intrinsic and bilayer graphene, *Phys. Rev. B* **83**, 085405 (2011).
- [17] P. K. Gogoi, I. Santoso, S. Saha, S. Wang, A. H. C. Neto, K. P. Loh, T. Venkatesan, and A. Rusydi, Optical conductivity study of screening of many-body effects in graphene interfaces, *Europhys. Lett.* **99**, 67009 (2012).
- [18] Y. C. Chang, C. H. Liu, C. H. Liu, Z. Zhong, and T. B. Norris, Extracting the complex optical conductivity of mono- and bilayer graphene by ellipsometry, *Appl. Phys. Lett.* **104**, 261909 (2014).
- [19] K. K. Tikuišis, A. Dubroka, K. Uhlířová, F. Speck, T. Seyller, M. Losurdo, M. Orlita, and M. Veis, Dielectric function of epitaxial quasi-freestanding monolayer graphene on Si-Face 6H-SiC in a broad spectral range, *Phys. Rev. Mater.* **7**, 044201 (2023).
- [20] A. N. Toksumakov *et al.*, Anomalous optical response of graphene on hexagonal boron nitride substrates, *Commun. Phys.* **6**, 13 (2023).
- [21] W. Li, G. Cheng, Y. Liang, B. Tian, X. Liang, L. Peng, A. R. Hight Walker, D. J. Gundlach, and N. V. Nguyen, Broadband optical properties of graphene by spectroscopic ellipsometry, *Carbon* **99**, 348 (2016).
- [22] V. G. Kravets, A. N. Grigorenko, R. R. Nair, P. Blake, S. Anissimova, K. S. Novoselov, and A. K. Geim, Spectroscopic ellipsometry of graphene and an exciton-shifted van Hove peak in absorption, *Phys. Rev. B* **81**, 155413 (2010).
- [23] G. Isić, Spectroscopic ellipsometry of few-layer graphene, *J. Nanophotonics* **5**, 051809 (2011).
- [24] A. Matković, U. Ralević, G. Isić, M. M. Jakovljević, B. Vasić, I. Milošević, D. Marković, and R. Gajić, Spectroscopic ellipsometry and the fano resonance modeling of graphene optical parameters, *Phys. Scr.* **T149**, 014069 (2012).
- [25] K. F. Mak, J. Shan, and T. F. Heinz, Seeing many-body effects in single- and few-layer graphene: Observation of two-dimensional saddle-point excitons, *Phys. Rev. Lett.* **106**, 046401 (2011).
- [26] J. W. Weber, V. E. Calado, and M. C. M. Van De Sanden, Optical constants of graphene measured by spectroscopic ellipsometry, *Appl. Phys. Lett.* **97**, 091904 (2010).
- [27] F. J. Nelson, V. K. Kamineni, T. Zhang, E. S. Comfort, J. U. Lee, and A. C. Diebold, Optical properties of large-area

- polycrystalline chemical vapor deposited graphene by spectroscopic ellipsometry, *Appl. Phys. Lett.* **97**, 253110 (2010).
- [28] K. F. Mak, M. Y. Sfeir, Y. Wu, C. H. Lui, J. A. Misewich, and T. F. Heinz, Measurement of the optical conductivity of graphene, *Phys. Rev. Lett.* **101**, 196405 (2008).
- [29] T. Kobayashi *et al.*, Production of a 100-m-long high-quality graphene transparent conductive film by roll-to-roll chemical vapor deposition and transfer process, *Appl. Phys. Lett.* **102**, 023112 (2013).
- [30] S. Zhang, Z. Li, and F. Xing, Review of polarization optical devices based on graphene materials, *Int. J. Mol. Sci.* **21**, 1608 (2020).
- [31] Y. Zhang, Y. Feng, B. Zhu, J. Zhao, and T. Jiang, Graphene based tunable metamaterial absorber and polarization modulation in terahertz frequency, *Opt. Express* **22**, 22743 (2014).
- [32] Q. Bao, H. Zhang, B. Wang, Z. Ni, C. H. Y. X. Lim, Y. Wang, D. Y. Tang, and K. P. Loh, Broadband graphene polarizer, *Nat. Photonics* **5**, 411 (2011).
- [33] M. Liu, X. Yin, E. Ulin-Avila, B. Geng, T. Zentgraf, L. Ju, F. Wang, and X. Zhang, A graphene-based broadband optical modulator, *Nature (London)* **474**, 64 (2011).
- [34] T. Mueller, F. Xia, and P. Avouris, Graphene photodetectors for high-speed optical communications, *Nat. Photonics* **4**, 297 (2010).
- [35] R. Hao, W. Du, H. Chen, X. Jin, L. Yang, and E. Li, Ultra-compact optical modulator by graphene induced electrorefraction effect, *Appl. Phys. Lett.* **103**, 061116 (2013).
- [36] Q. Ye, J. Wang, Z. Liu, Z.-C. Deng, X.-T. Kong, F. Xing, X.-D. Chen, W.-Y. Zhou, C.-P. Zhang, and J.-G. Tian, Polarization-dependent optical absorption of graphene under total internal reflection, *Appl. Phys. Lett.* **102**, 021912 (2013).
- [37] J. Yang, D. Chen, J. Zhang, Z. Zhang, and J. Huang, Polarization modulation based on the hybrid waveguide of graphene sandwiched structure, *Europhys. Lett.* **119**, 54001 (2017).
- [38] R. Wang, D. Li, H. Wu, M. Jiang, Z. Sun, Y. Tian, J. Bai, and Z. Ren, All-optical intensity modulator by polarization-dependent graphene-microfiber waveguide, *IEEE Photonics J.* **9**, 7105708 (2017).
- [39] N. A. Malik, P. Nicolosi, K. Jimenez, A. Gaballah, A. Giglia, M. Lazzarino, and P. Zuppella, Experimental study of few-layer graphene: Optical anisotropy and pseudo-Brewster angle shift in vacuum ultraviolet spectral range, *Adv. Photonics Res.* **2**, 2000207 (2021).
- [40] A. Matković, U. Ralević, M. Chhikara, M. M. Jakovljević, D. Jovanović, G. Bratina, and R. Gajić, Influence of transfer residue on the optical properties of chemical vapor deposited graphene investigated through spectroscopic ellipsometry, *J. Appl. Phys.* **114**, 093505 (2013).
- [41] M. Houmad, H. Zaari, A. Benyoussef, A. El Kenz, and H. Ez-Zahraouy, Optical conductivity enhancement and band gap opening with silicon doped graphene, *Carbon* **94**, 1021 (2015).
- [42] M. A. El-Sayed *et al.*, Optical constants of chemical vapor deposited graphene for photonic applications, *Nanomaterials* **11**, 1230 (2021).
- [43] Y. Y. Wang, Z. H. Ni, T. Yu, Z. X. Shen, H. M. Wang, Y. H. Wu, W. Chen, and A. T. S. Wee, Raman studies of monolayer graphene: The substrate effect, *J. Phys. Chem. C* **112**, 10637 (2008).
- [44] C. Jia, J. Jiang, L. Gan, and X. Guo, Direct optical characterization of graphene growth and domains on growth substrates, *Sci. Rep.* **2**, 707 (2012).
- [45] J. Hass, F. Varchon, J. E. Millán-Otoya, M. Sprinkle, N. Sharma, W. A. De Heer, C. Berger, P. N. First, L. Magaud, and E. H. Conrad, Why multilayer graphene on 4H-SiC(000 $\bar{1}$) behaves like a single sheet of graphene, *Phys. Rev. Lett.* **100**, 125504 (2008).
- [46] W. Zhu, V. Perebeinos, M. Freitag, and P. Avouris, Carrier scattering, mobilities, and electrostatic potential in monolayer, bilayer, and trilayer graphene, *Phys. Rev. B* **80**, 235402 (2009).
- [47] E. H. Hwang, S. Adam, and S. Das Sarma, Carrier transport in two-dimensional graphene layers, *Phys. Rev. Lett.* **98**, 186806 (2007).
- [48] S. Nannarone, The bear beamline at elettra, *AIP Conf. Proc.* **705**, 450 (2004).
- [49] H. Fujiwara, *Spectroscopic Ellipsometry: Principles and Applications* (Wiley, Chichester, UK, 2007).
- [50] T. C. Asmara *et al.*, Mechanisms of charge transfer and redistribution in LaAlO₃/SrTiO₃ revealed by high-energy optical conductivity, *Nat. Commun.* **5**, 3663 (2014).
- [51] T. C. Asmara, I. Santoso, and A. Rusydi, Self-consistent iteration procedure in analyzing reflectivity and spectroscopic ellipsometry data of multilayered materials and their interfaces, *Rev. Sci. Instrum.* **85**, 123116 (2014).
- [52] I. Santoso, S. L. Wong, X. Yin, P. K. Gogoi, T. C. Asmara, H. Huang, W. Chen, A. T. S. Wee, and A. Rusydi, Optical and electronic structure of quasi-freestanding multilayer graphene on the carbon face of SiC, *Europhys. Lett.* **108**, 37009 (2014).
- [53] Y. W. Sun, D. Holec, D. Gehringer, L. Li, O. Fenwick, D. J. Dunstan, and C. J. Humphreys, Graphene on silicon: Effects of the silicon surface orientation on the work function and carrier density of graphene, *Phys. Rev. B* **105**, 165416 (2022).
- [54] U. Fano, Effects of configuration interaction on intensities and phase shifts, *Phys. Rev.* **124**, 1866 (1961).
- [55] L. Fleming, M. D. Ulrich, K. Efimenko, J. Genzer, A. S. Y. Chan, T. E. Madey, S.-J. Oh, O. Zhou, and J. E. Rowe, Near-Edge absorption fine structure and UV photoemission spectroscopy studies of aligned single-walled carbon nanotubes on Si(100) substrates, *J. Vac. Sci. Technol., B* **22**, 2000 (2004).
- [56] C. D. Spataru, S. Ismail-Beigi, L. X. Benedict, and S. G. Louie, Excitonic effects and optical spectra of single-walled carbon nanotubes, *Phys. Rev. Lett.* **92**, 077402 (2004).
- [57] F. Wang, D. J. Cho, B. Kessler, J. Deslippe, P. J. Schuck, S. G. Louie, A. Zettl, T. F. Heinz, and Y. R. Shen, Observation of excitons in one-dimensional metallic single-walled carbon nanotubes, *Phys. Rev. Lett.* **99**, 227401 (2007).
- [58] J. Deslippe, C. D. Spataru, D. Prendergast, and S. G. Louie, Bound excitons in metallic single-walled carbon nanotubes, *Nano Lett.* **7**, 1626 (2007).
- [59] M. Rohlfing and S. G. Louie, Electron-hole excitations and optical spectra from first principles, *Phys. Rev. B* **62**, 4927 (2000).